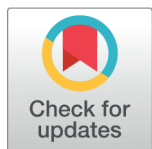


RESEARCH ARTICLE



Structural, Dielectric Properties and Conduction Mechanism of SrBi₄Ti₄O₁₅ Ceramics

Chitta Lakshmipathi^{1*}, Borra Rajesh Kumar², Kande Sreelekha³,
Thota Subba Rao¹

¹ Department of Physics, Sri Krishnadevaraya University, Anantapur, 515003, Andhra Pradesh, India

² Department of Physics, GITAM (Deemed to be University), Visakhapatnam, 530045, Andhra Pradesh, India

³ Department of Physics, Government Degree College (Autonomous), Anantapur, 515001, Andhra Pradesh, India



Received: 28-02-2022

Accepted: 10-07-2022

Published: 26-08-2022

Citation: Lakshmipathi C, Rajesh Kumar B, Sreelekha K, Rao TS (2022) Structural, Dielectric Properties and Conduction Mechanism of SrBi₄Ti₄O₁₅ Ceramics. Indian Journal of Science and Technology 15(33): 1605-1612. <https://doi.org/10.17485/IJST/v15i33.488>

* Corresponding author.

sreelakshmipathisku@gmail.com

Funding: None

Competing Interests: None

Copyright: © 2022 Lakshmipathi et al. This is an open access article distributed under the terms of the [Creative Commons Attribution License](#), which permits unrestricted use, distribution, and reproduction in any medium, provided the original author and source are credited.

Published By Indian Society for Education and Environment ([iSee](#))

ISSN

Print: 0974-6846

Electronic: 0974-5645

Abstract

Objectives: 1. To prepare SrBi₄Ti₄O₁₅ ceramics via solid-state reaction method. 2. To make a systematic investigations on structural and dielectric properties of SBT ceramics. **Methods:** The structural information of Strontium Bismuth Titanate (SBT) ceramics is examined by X-ray diffraction and Raman spectroscopy techniques. The surface morphology and elemental analysis of SBT ceramic is employed by scanning electron microscope attached with energy-dispersive X-ray spectroscopy. The dielectric measurements of SBT ceramics were performed using the impedance analyzer HIOKI-3532 LCR meter. **Findings:** From the X-ray diffraction studies, SBT exhibits a strongest diffraction peak (1 1 9) with the lattice parameters $a = 5.428 \text{ \AA}$, $b = 5.423 \text{ \AA}$, and $c = 42.146 \text{ \AA}$. The diffraction patterns were indexed to the orthorhombic phase. The surface morphology of the samples shows plate-like morphology with a grain size of $\sim 1 \mu\text{m}$. The temperature-dependent ac conductivity confirms the thermally activated conduction mechanism. The ac conductivity of SBT ceramic was increased from 2.25×10^{-5} to $7.16 \times 10^{-4} \Omega \cdot \text{m}^{-1}$ with an increase of frequency from 10 kHz to 1 MHz. The high curie temperature at $\sim 540 \text{ }^\circ\text{C}$, and low dielectric loss of ~ 0.031 for SBT ceramics can be appropriate for high-temperature electronic applications. **Novelty:** SBT ceramic exhibits enhanced electrical conductivity value ($7.16 \times 10^{-4} \Omega \cdot \text{m}^{-1}$) and makes it suitable for electronic device applications.

Keywords: Scanning electron microscope; Dielectric constant; Dielectric loss; Conduction mechanism 1; X-ray diffraction

1 Introduction

Strontium Bismuth Titanate SrBi₄Ti₄O₁₅ (SBT) belongs to the bismuth oxide layer structure ferroelectrics (BLSF) with potential applications in ferroelectric non-volatile RAM, memory storage devices, high-temperature piezo-electrics, actuators, and sensor

applications. The piezoelectric properties of SBT ceramic are poor compared to the lead-based system. SBT ceramic has an orthorhombic structure (space group: $A2_1am$) and above the Curie temperature $T_c=530^\circ\text{C}$, it changes to a tetragonal structure (space group: $I4/mmm$)^(1–4). The Bi and oxygen vacancies will be formed for SBT ceramics during the process of sintering, the oxygen vacancy maintains the neutral charge^(5,6). The oxygen vacancy may cause due to enhanced leakage current, impeding the displacement of the Ti^{4+} ion, screening the electric field near the space charge region, and trapping of charge carriers^(7,8). To reduce the defects such as poor density and electrical properties in SBT ceramics, controlling the sintering process temperature leads to lowering the volatilization of Bi_2O_3 . For memory device applications, it is necessary for a material with high fatigue, low dielectric loss, and conductivity. Some previous literature reported that substituting the A and/or B-site of SBT will improve the ferroelectric properties and minimize the oxygen vacancies^(9,10). The effect of oxide additives like Gd_2O_3 , CeO_2 , MnO_2 , and Cr_2O_3 on the phase structures and electrical properties of SBT ceramics were investigated by Shaozhao Wang et al.⁽¹¹⁾. The oxide additives improve the piezoelectric property of SBT ($d_{33} = 10$ pC/N); SCBT-Cr and SGBT-Cr obtained a higher d_{33} of 26 pC/N and 28 pC/N, respectively. Among the various compositions, $\text{Sr}_{0.92}\text{Gd}_{0.053}\text{Bi}_4\text{Ti}_4\text{O}_{15} + 0.2$ wt% Cr_2O_3 presented the best electrical properties with $T_c = 555^\circ\text{C}$, $\tan \delta = 0.4\%$, $k_p = 6.35\%$, $d_{33} = 28$ pC/N, and good thermally stable piezoelectricity. Recently, Vipul Kumar Sharma et al.⁽¹²⁾ synthesized the bismuth layered ferroelectrics (BLFs) $\text{BaBi}_4\text{Ti}_4\text{O}_{15}$ and $\text{SrBi}_4\text{Ti}_4\text{O}_{15}$ using solid-state reaction technique. The thermal etching post-sintering enhances the dielectric constant for $\text{BaBi}_4\text{Ti}_4\text{O}_{15}$, but significantly decreases $\text{SrBi}_4\text{Ti}_4\text{O}_{15}$. At 10 MHz, $\sim 110^\circ\text{C}$ rise in transition temperature and ten times reduction in dielectric constant is observed.

The novel properties like high transition (Curie) temperature and a low dielectric loss made this material attractive to current science. The present work aims to study the mechanisms leading to enhancing the electrical properties of SBT ceramics, and the analysis will be beneficial for high-temperature electronic applications. The structural, dielectric behavior and the conduction mechanism of SBT ceramics prepared via the solid-state reaction technique will be discussed.

2 Methodology

$\text{SrBi}_4\text{Ti}_4\text{O}_{15}$ (SBT) ceramic was prepared via the conventional solid-state reaction route as shown in Figure 1. The high purity (99.9%) analytical grade metal oxides of Bi_2O_3 , SrCO_3 , and TiO_2 (Sigma-Aldrich) were used as the starting materials. The stoichiometric amounts of the oxide mixtures were grinded in a ball miller (Retsch PM-400, Germany). These oxides were thoroughly grinded in Teflon jars in the presence of acetone medium at 300 rpm for 12 hours. After ball milling, the obtained slurry was heated at 70°C in a hot air oven, and finally, the mixture was calcinated at 950°C for 4 hours in an alumina crucible with a heating rate of $10^\circ\text{C}/\text{min}$. The powders were ball milled again for 12 hours with zirconia balls in the ratio of 1:10, the dried powders were mixed with 3% of PVA which acts as a binder. Finally, these were pressed into circular compact disks with a dimension of 2 mm thickness and 10 mm diameter at 250 MPa. These pellets were sintered at 1100°C using a conventional programmable furnace with a heating rate of $5^\circ\text{C}/\text{min}$ for 2 hours. The crystal structure of SBT ceramics was characterized by an X-ray diffractometer (XRD) (Bruker D8 Advanced) using $\text{CuK}\alpha$ radiation in the range $2\theta = 10\text{--}80^\circ$ with a step size of 0.02° . Raman scattering measurements were performed using a Raman spectrometer (Model: LabRAM HR800, Horiba Jobin Yvon) with a source of excitation at a 514.5 nm line of an argon laser (output power of 200 mW and laser spot power was < 20 mW). The morphology and microstructure of SBT ceramic is examined using the scanning electron microscope (SEM). The elemental analysis of the SBT ceramic is measured from the energy dispersive spectroscopy (EDS) attached with SEM. The electrical properties of the sintered pellets were silver coated and heated at 300°C for 2 hours. The dielectric properties of SBT ceramic is measured at frequencies of 10 kHz -1MHz from 30°C (RT) to 570°C with a heating rate of $2^\circ\text{C}/\text{min}$ using the HIOKI 3532 LCR meter interfaced to a computer.

3 Results and Discussion

X-ray diffraction (XRD) profile of strontium bismuth titanate (SBT) ceramic is shown in Figure 2. No secondary phases were observed in the XRD pattern. The peaks were well matched with the JCPDS F.No. 43-0973 and indexed to orthorhombic phase ($A2_1am$ space group). The maximum diffraction peak intensity is (1 1 9) reflection, the most intense reflection of BLSF compounds of (1 1 2m+1). From XRD spectra, no additional peaks related to any secondary phase were observed in SBT ceramics. XRD patterns confirm the BiO layer-type structure with $m=4$. By using the CHEKCELL software within the error limit of $\pm 0.002\text{\AA}$, lattice parameters were calculated as $a=5.428\text{\AA}$, $b=5.423\text{\AA}$ and $c=42.146\text{\AA}$, Volume (V)= 1240.7\AA^3 , orthorhombic distortion given as $2(a-b)/(a+b)$ is 0.0098. The density of the SBT ceramic measured via the Archimedes method was 97.4%.

The scanning electron micrographs of $\text{SrBi}_4\text{Ti}_4\text{O}_{15}$ ceramic is shown in Figure 3(a). The surface morphology looks like a highly anisotropic microstructure with plate-like grains. These grains are formed because of the growth along a–b plane faster than the c-axis in BLSFs. The larger grain size from the surface morphology enhances the piezoelectric properties of the

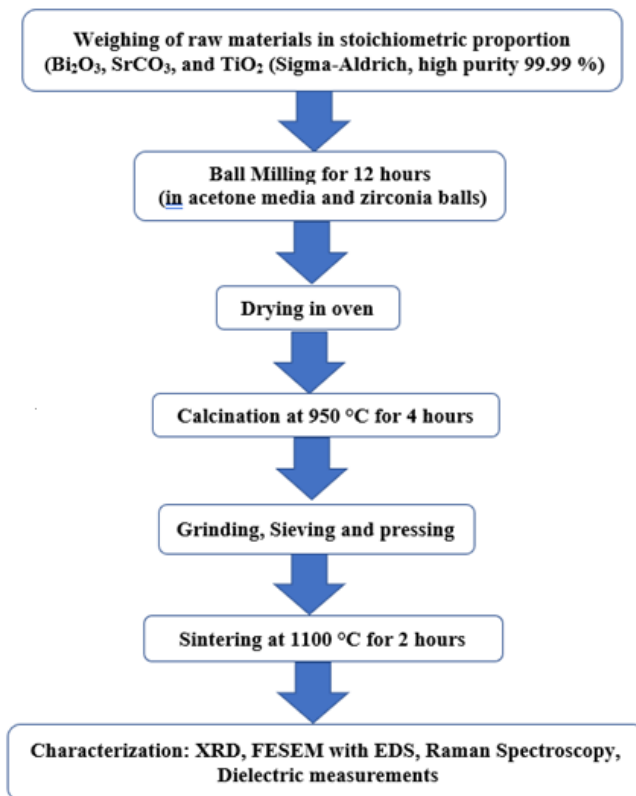
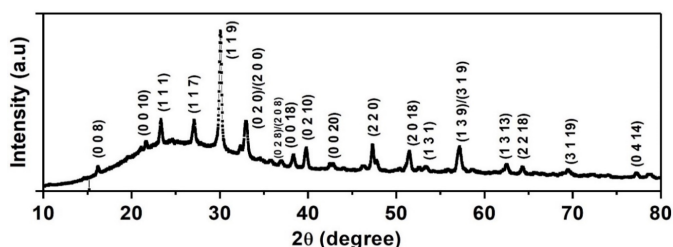


Fig 1. Flow chart for preparing SBT ceramics

Fig 2. XRD pattern of SrBi₄Ti₄O₁₅ ceramic

ceramics.

The EDS spectra are shown in Figure 3(b)-(g) confirm the presence of the elements Sr, Bi, Ti, and O. The atomic percentage of Sr, Bi, Ti, and O elements in 8.01%, 23.03%, 21.29%, and 47.67% respectively. The elemental mapping for SBT ceramic is homogeneous with a slight variation in the stoichiometry may be due to Bi volatilization and loss at the high-temperature sintering process.

The room temperature Raman scattering spectra of SrBi₄Ti₄O₁₅ ceramic compound is shown in Figure 4. The SBT ceramic exhibits phonon modes around 118, 270, 560, and 866 cm⁻¹, which belong to the orthorhombic structure (space group of A2₁am). The phonon modes observed in the spectra matched well with the previously reported literature data on SBT ceramics reported as the single-phase material⁽¹³⁾. The lower frequency phonon modes are due to the motion of Bi³⁺ ions at the A-site, which was noticed in the ABi₄Ti₄O₁₅ (A = Sr, Ba, Ca, and Pb) layered structures. The frequency modes >200 cm⁻¹ are related to Ti-O bonds, mode at 272 cm⁻¹ belongs to B_{1g} mode and torsional bending of TiO₆ octahedra. The mode at 560 cm⁻¹ belongs to the oxygen atoms of octahedra, and the phonon mode at 866 cm⁻¹ is assigned to the symmetric stretching of TiO₆ octahedra.

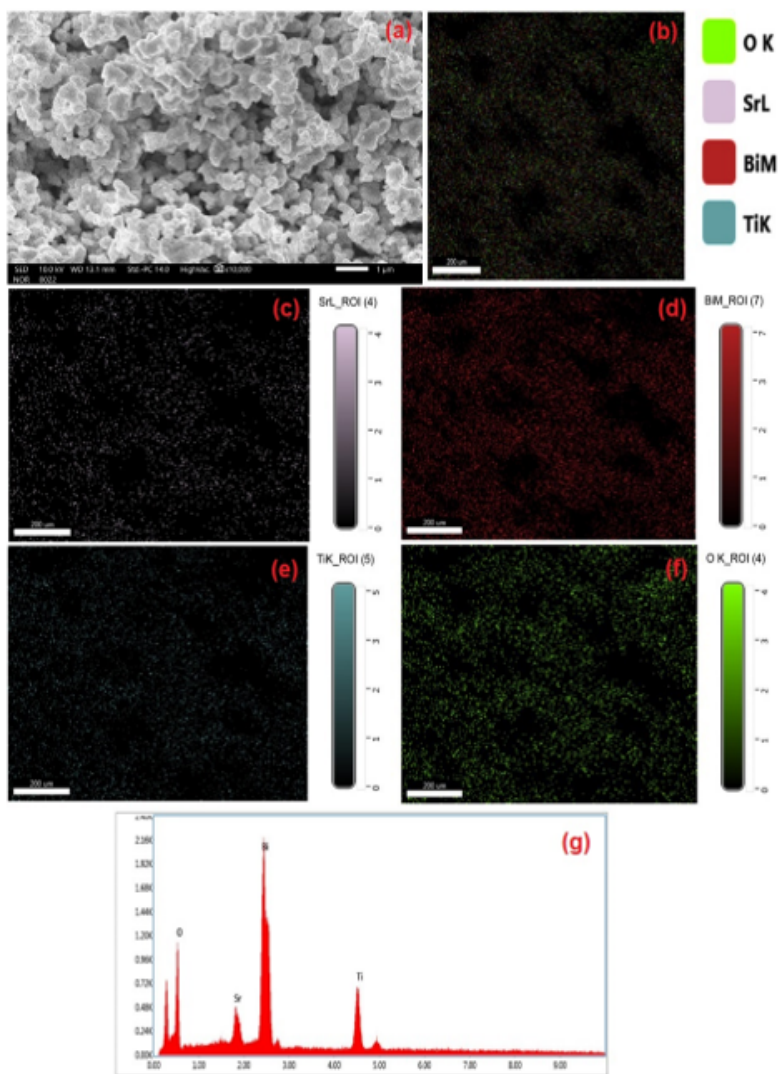


Fig 3. FESEM-EDS elemental mapping of $\text{SrBi}_4\text{Ti}_4\text{O}_{15}$ (a) secondary electron image and elemental mapping, (b) all the elements in SBT ceramic, (c) Sr, (d) Bi, (e) Ti, (f) O elements, and (g) Energy dispersive spectra

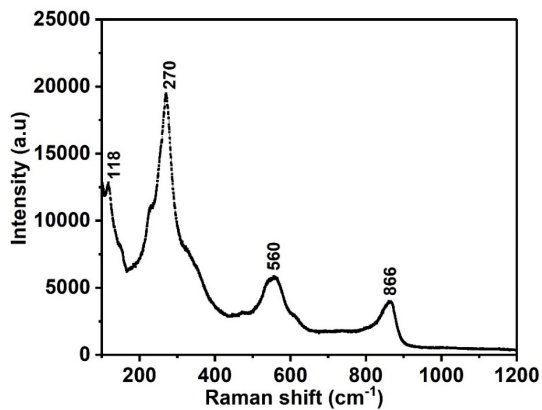


Fig 4. Raman spectroscopy of SBT ceramic

The dielectric constant measurements for SrBi₄Ti₄O₁₅ ceramic at different frequencies with the variation of temperature from 30 °C to 570 °C is shown in Figure 5. The Curie temperature (T_c) for SBT is observed at 540 °C. Above the T_c, decrement of dielectric constant with the increment of temperature signifying the transition from ferroelectric to paraelectric phase. These results were in good agreement with the work done by Lei Yu et al.⁽¹⁴⁾. The high dielectric constant values at lower frequencies may be due to the accumulating charges at the material conducting surface regions, which leads to polarization. The charges do not accumulate at higher frequencies, which decreases the dielectric constant. With the increase of frequency, the carriers gain energy, and a few carriers break the grain boundary and enter the grain portion of the material. At very high frequencies, the dielectric constant values of SBT are decreased with the increase of frequency. This may also be due to the breakage of grain boundaries by the cloud of charge carriers⁽¹⁵⁾. The temperature variation of dielectric loss tangent (tan δ) for SBT ceramic is shown in Figure 6. The dielectric loss tangent (tan δ) values at room temperature for the frequencies 10 kHz, 100 kHz, and 1 MHz are 0.031, 0.065, and 0.084, respectively. The dielectric tangent loss values are low at a temperature <500 °C. When the temperature exceeds the Curie temperature, the dielectric loss sharply increases because of the increment in the thermally conductive current, which can be attributed to the creation of oxygen vacancies⁽¹⁶⁾. The lower values of tan δ will be beneficial for designing the high signal-to-noise ratio pyroelectric device.

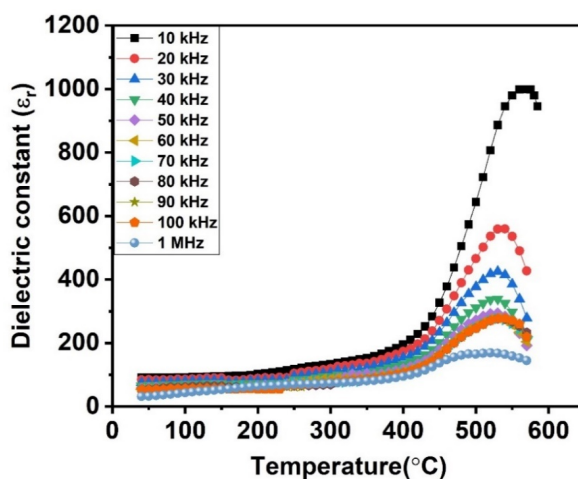


Fig 5. Variation of dielectric constant with temperature for SBT

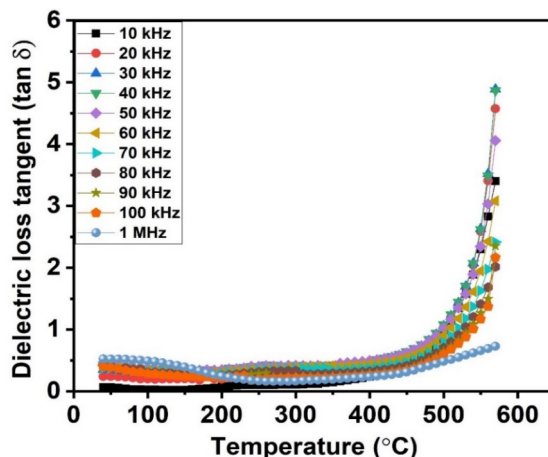


Fig 6. Variation of tan δ with temperature for SBT.

The modified Curie–Weiss law is given as below

$$1/\epsilon_r = 1/\epsilon_m + [(T-T_c)^{-1}/C] \quad (1)$$

where γ and C are constants providing the characteristic features of the phase transition. The values of $\gamma = 1$ and 2 represent the behavior of normal Curie-Weiss law and phase transition diffuseness. The plotting of $\log(1/\epsilon_r - 1/\epsilon_m)$ versus $\log(T - T_c)$ for SBT ceramic measured at the frequency of 100 kHz is illustrated in Figure 7. The plot was linear with a γ value of 1.882 ± 0.002 , indicating the ferroelectric nature of SBT ceramic. The observed γ value represents the disordered structure in the arrangement of cations regarding the crystallographic site, and fluctuations in the composition may cause diffuseness.

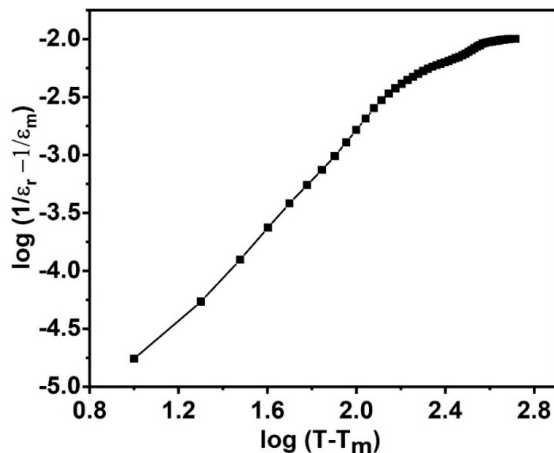


Fig 7. Plot of $\log(1/\epsilon_r - 1/\epsilon_m)$ versus $\log(T - T_m)$ for SBT ceramic at 100 kHz.

The ac conductivity with the temperature variation provides relaxation conduction mechanisms⁽¹⁷⁾. The ac conductivity for SBT ceramic is determined from the equation

$$\sigma_{ac} = \epsilon_o \epsilon_r \omega \tan \delta \quad (2)$$

where ϵ_o , ν , ϵ_r , and $\tan \delta$ is the free space permittivity, frequency, relative permittivity, and dielectric loss. The ac conductivity values are fitted with Jonscher's universal power law as given below

$$\sigma_{ac} = \sigma_{dc} + A\omega^s \quad (3)$$

where σ_{dc} , A, and s represent dc conductivity, pre-exponential factor, and frequency exponent. By fitting equation (3), the values of exponent s, σ_{dc} , and A are found to be 0.88, $6.46 \times 10^{-4} \Omega^{-1} \cdot m^{-1}$, and 2.18×10^7 , respectively and the linear correlation coefficient R^2 is obtained as 0.991. The frequency exponent (s) value in SBT ceramic is < 1 , representing the non-Debye behavior and translational motion of charge carriers with the hopping mechanism. The strength of the polarizability will be determined by the pre-exponential factor 'A'. The ac conductivity of SBT ceramics increased from 2.25×10^{-5} to $7.16 \times 10^{-4} \Omega \cdot m^{-1}$ with an increase of frequency from 10 kHz to 1 MHz. The increase in conductivity with frequency indicates that the charge carriers are bound and trapped in the defects, unlike the free carriers. The ac conductivity (σ_{ac}) variation with temperature for SBT ceramic is shown in Figure 8. The increasing trend of electrical conductivity of SBT ceramic as a function of temperature and frequency indicates the enhancement of the hopping rate of charge carriers between the localized cations⁽¹⁸⁾. The conductivity enhancement at higher temperatures is because of hopping charge carriers and oxygen vacancies. At lower temperatures, the ac conductivity is independent of temperature, with the space charges leading to the conduction mechanism. The activation energy values of SBT ceramics are estimated from the Arrhenius relation

$$\sigma_{ac} = \sigma_o e^{-E_a/k_B T} \quad (4)$$

where A, E_a , and k_B represent the pre-exponential factor, activation energy, and Boltzmann constant. The activation energy (E_a) values are estimated from the linear least-square fitting of ac conductivity data obtained from equation (3). The conduction activation energies $< T_c$ were in the range of 0.34 - 0.91 eV and $> T_c$ in the range of 0.61 - 1.38 eV. The activation energy decreases with increased frequency, suggesting the hopping of charge carriers. These activation energy values are well in agreement with the values associated with singly/doubly ionized oxygen vacancies in layered perovskite ferroelectric oxide materials⁽⁴⁾.

QMT (quantum mechanical tunneling) model is associated with when s is temperature independent, CBH (correlated barrier hopping) model associates when s decreases with temperature, SP (small polaron hopping) the parameter 's' increases with temperature. In the overlapping large-polaron (OLP model), 's' decreases with the temperature reaching the lower value and then raises. The frequency exponent expression based on the CBH model can be determined from the relation

$$s = 1 - [6k_B T / (W_m - k_B T \ln(1/\omega\tau_o))] \quad (5)$$

where k_B , T, τ_o , and W_m represent Boltzmann's constant, temperature, relaxation time, and maximum barrier height. When $TW_m \gg k_B T \ln(1/\omega\tau_o)$, the equation (5) is related as

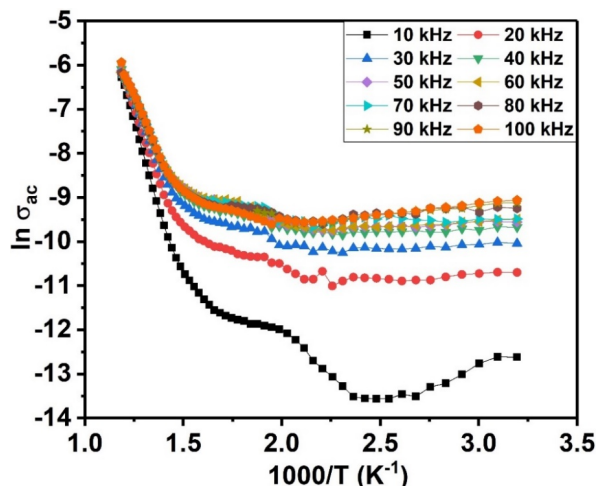


Fig 8. $\ln \sigma_{ac}$ vs $10^3/T$ for SBT ceramic.

$$s = [1 - (6k_B T / W_m)] \quad (6)$$

The value of s and T ($=303K$) is substituted in the equation (6), W_m is obtained as 1.31 eV, which is matched well with activation energy values ranging from 0.34 to 1.38 eV of double ionized oxygen vacancies (V_o^{**}), which confirms the CBH conduction mechanism. The minimum hopping distance (R_{min}) is determined from the equation

$$R_{min} = 2e^2 / \pi \epsilon \epsilon_o W_m \quad (7)$$

where ϵ_o and ϵ are the permittivity of free space and dielectric constant. The corresponding curve of R_{min} is shown in Figure 9, which shows that the hopping distance increased with increasing frequency. Based on the CBH model and Austin-Mott formula, the ac conductivity (σ_{ac}) related to the density of localized states $N(E_F)$ with the Fermi level is given as

$$\sigma_{ac}(\omega) = (\pi/3) e^2 \omega k_B T (N(E_F))^2 \alpha^{-5} (\ln f_o / \omega)^4 \quad (8)$$

where e , f_o , and α are the charge of an electron, photon frequency, and localized wave function. The density of localized states $N(E_F)$ is calculated from the equation (8) by assuming $f_o = 10^{13}$ Hz, $\alpha = 10^{10} \text{ m}^{-1}$. The dependence of $N(E_F)$ with frequency for SBT ceramic is shown in Figure 9.

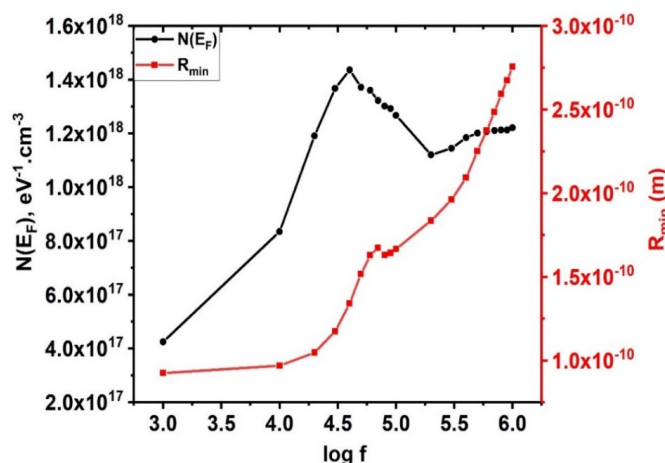


Fig 9. Variation of $N(E_F)$ and R_{min} with frequency for SBT ceramic.

$N(E_F)$ value increases with frequency up to 40 kHz. The higher $N(E_F)$ values indicate the hopping between the pair sites that dominate the charge transport mechanism. Above the frequency of 40 kHz, the $N(E_F)$ decreases due to increased thermal activation energy for electrical conduction. The decrease of $N(E_F)$ is correlated with an increase in the hopping distance between the localized states of the charge carriers.

4 Conclusion

SBT ceramics were prepared by a solid-state reaction route. XRD pattern exhibits a single orthorhombic phase with a space group of $A2_1am$. SBT ceramics show a plate-like morphology due to the highly anisotropic layered structure. The dielectric constant values measured at the frequencies 10 kHz, 100 kHz, and 1 MHz are 178, 54, and 32. The dielectric constant and dielectric loss stabilize at higher frequencies due to the variation in an electric field, making it too rapid to follow molecular dipoles. The contribution towards polarization decreases because of internal frictional forces. The temperature variation of ac conductivity shows that the conduction mechanism is thermally activated. The activation energy values of SBT ceramic estimated from the ac conductivity are consistent with the BSLF compounds, which indicates the conduction mechanism is due to doubly ionized oxygen vacancies. The high dielectric constant ~ 178 at room temperature, transition temperature $T_c \sim 540^\circ\text{C}$, and low dielectric loss ~ 0.031 of SBT ceramic could be demonstrated as a beneficial candidate for high-temperature electronic applications.

5 Acknowledgement

A part of this research work was performed using the facilities available at CeNSE, funded by MeitY, Govt. of India, at IISc., Bengaluru

References

- 1) Wu Y, Zhao X, Zhang Z, Xiang J, Suo H, Guo C. Dual-mode dichromatic $\text{SrBi}_4\text{Ti}_4\text{O}_{15}$: Er^{3+} emitting phosphor for anti-counterfeiting application. *Ceramics International*. 2021;47(11):15067–15072. Available from: <https://doi.org/10.1016/j.ceramint.2021.02.064>.
- 2) Uppala R, Zacharias E, Anand G, Sarah P. Modelling of Dielectric Studies on Rare-Earth Substituted Strontium Bismuth Titanate Using Modified Lorentz Equation. *Integrated Ferroelectrics*. 2021;221(1):245–253. Available from: <https://doi.org/10.1080/10584587.2021.1965831>.
- 3) Nayak P, Nayak SK, Badapanda T. Piezoelectricity and excellent thermal stability in W^{6+} modified $\text{SrBi}_4\text{Ti}_4\text{O}_{15}$ ceramics. *AIP Conference Proceedings*. 2020;2265:030018. Available from: <https://doi.org/10.1063/5.0017189>.
- 4) Rambabu A, Raju KCJ. Impact of Sm-substitution and microwave sintering on dielectric and mechanical properties of $\text{SrBi}_4\text{Ti}_4\text{O}_{15}$ ceramics. *Journal of Materials Science: Materials in Electronics*. 2020;31(22):19698–19712. Available from: <https://doi.org/10.1007/s10854-020-04496-z>.
- 5) Babu BS, Prasad G, Kumar GS, Prasad NV. Studies on samarium modified $\text{SrBi}_{4-x}\text{Sm}_x\text{Ti}_4\text{O}_{15}$ Aurivillius ferroelectric ceramics. *Ferroelectrics*. 2021;572(1):106–117. Available from: <https://doi.org/10.1080/00150193.2020.1868876>.
- 6) Wang S, Zhou H, Wu D, Li L, Chen Y. Effects of Oxide Additives on the Phase Structures and Electrical Properties of $\text{SrBi}_4\text{Ti}_4\text{O}_{15}$ High-Temperature Piezoelectric Ceramics. *Materials*. 2020;14(20):6227–6227. Available from: <https://doi.org/10.3390/ma14206227>.
- 7) Ravikiran U, Sarah P, Zacharias E. Electrical studies on Na and Sm substituted strontium bismuth titanate (SBTi) ceramics. *Ferroelectrics*. 2021;571(1):61–75. Available from: <https://doi.org/10.1080/00150193.2020.1853740>.
- 8) Wang Y, Liu H, Yan T, Zhao J, Li J, Guo S, et al. Significantly reduced conductivity in strontium titanate-based lead-free ceramics by excess bismuth. *Materials Letters*. 2022;309:131453–131453. Available from: <https://doi.org/10.1016/j.matlet.2021.131453>.
- 9) Elfadl AA, Bashal AH, Althobaiti MG. A Study on Dielectric Permittivity, Structure, and AC Conductivity of Zinc and Copper Doped Bentonite Composites. *Journal of Inorganic and Organometallic Polymers and Materials*. 2022;32(1):191–199. Available from: <https://doi.org/10.1007/s10904-021-02112-z>.
- 10) Liu F, Jiang X, Chen C, Nie X, Huang X, Chen Y, et al. Structural, electrical and photoluminescence properties of Er^{3+} -doped $\text{SrBi}_4\text{Ti}_4\text{O}_{15}$ — $\text{Bi}_4\text{Ti}_3\text{O}_{12}$ inter-growth ceramics. *Frontiers of Materials Science*. 2019;13(1):99–106. Available from: <https://doi.org/10.1007/s11706-019-0454-3>.
- 11) Wang S, Zhou H, Wu D, Li L, Chen Y. Effects of Oxide Additives on the Phase Structures and Electrical Properties of $\text{SrBi}_4\text{Ti}_4\text{O}_{15}$ High-Temperature Piezoelectric Ceramics. *Materials*. 2021;14(20):6227–6227. Available from: <https://doi.org/10.3390/ma14206227>.
- 12) Sharma VK, Nathawat R, Rathore SS. Dielectric properties correlation with microstructure in $\text{ABi}_{4-x}\text{Ti}_4\text{O}_{15}$ ($A = \text{Sr}, \text{Ba}$) bismuth layered ferroelectrics. *Materials Advances*. 2022;3(12):4890–4898. Available from: <https://doi.org/10.1039/D2MA00333C>.
- 13) Kotb HM, Ahmad MM, Ansari SA, Kayed TS, Alshoaibi A. Dielectric Properties of Colossal-Dielectric-Constant $\text{Na}_{1/2}\text{La}_{1/2}\text{Cu}_3\text{Ti}_4\text{O}_{12}$ Ceramics Prepared by Spark Plasma Sintering. *Molecules*. 2022;27(3):779–779. Available from: <https://doi.org/10.3390/molecules27030779>.
- 14) Yu L, Hao J, Li W, Fu P, Sun W, Chen C, et al. Strong red emission and enhanced electrical properties in Pr-doped $\text{SrBi}_4\text{Ti}_4\text{O}_{15}$ multifunctional ceramics. *Journal of Materials Science: Materials in Electronics*. 2019;30(19):17890–17898. Available from: <https://doi.org/10.1007/s10854-019-02141-y>.
- 15) Kumar NS, Suvarna RP, Naidu KCB. Negative dielectric behavior in tetragonal $\text{La}_{0.8}\text{Co}_{0.2-x}\text{Eu}_x\text{TiO}_3$ ($x = 0.01-0.04$) nanorods. *Materials Characterization*. 2020;166(8):110425–110425. Available from: <https://doi.org/10.1016/j.matchar.2020.110425>.
- 16) Ravikiran U, Sarah P, Suresh MB, Zacharias E. Effect of Sm and Na substitution on dielectric properties of $\text{SrBi}_{4-x}\text{Ti}_4\text{O}_{15}$. *Ferroelectrics*. 2018;537(1):237–245. Available from: <https://doi.org/10.1080/00150193.2018.1528947>.
- 17) Jose R, P V, Rafiq MA. Investigation into defect chemistry and relaxation processes in niobium doped and undoped $\text{SrBi}_{4-x}\text{Ti}_4\text{O}_{15}$ using impedance spectroscopy. *RSC Advances*;8(60):34437–34448. Available from: <https://doi.org/10.1039/C8RA06621C>.
- 18) Kumar NS, Suvarna RP, Naidu KCB. Grain and grain boundary conduction mechanism in sol-gel synthesized and microwave heated $\text{Pb}_{0.8-y}\text{La}_y\text{Co}_0.2\text{TiO}_3$ ($y = 0.2-0.8$) nanofibers. *Materials Chemistry and Physics*. 2019;223:241–248. Available from: <https://doi.org/10.1016/j.matchemphys.2018.11.004>.